AGU PUBLICATIONS

JGR

Journal of Geophysical Research: Space Physics

RESEARCH ARTICLE

10.1002/2014JA019832

Key Points:
- Coordinated observations made by five Fabry-Perot interferometers are shown
- An unexpected strong and sustained vertical thermospheric wind is observed
- The vertical wind is interpreted to be due to spectral contamination

Supporting Information:
- Readme
- Animation S1

Correspondence to:
J. J. Makela,
jmakela@illinois.edu

Citation:
Makela, J. J., et al. (2014), Storm time response of the midlatitude thermosphere: Observations from a network of Fabry-Perot interferometers, *J. Geophys. Res. Space Physics*, *119*, 6758–6773, doi:10.1002/2014JA019832.

Received 27 JAN 2014
Accepted 23 JUL 2014
Accepted article online 29 JUL 2014
Published online 12 AUG 2014

Storm time response of the midlatitude thermosphere: Observations from a network of Fabry-Perot interferometers

Jonathan J. Makela[1], Brian J. Harding[1], John W. Meriwether[2], Rafael Mesquita[2], Samuel Sanders[2], Aaron J. Ridley[3], Michael W. Castellez[4], Marco Ciocca[5], Gregory D. Earle[6], Nathaniel A. Frissell[6], Donald L. Hampton[7], Andrew J. Gerrard[8], John Noto[9], and Carlos R. Martinis[10]

[1]Department of Electrical and Computer Engineering, University of Illinois at Urbana-Champaign, Urbana, Illinois, USA, [2]Department of Physics and Astronomy, Clemson University, Clemson, South Carolina, USA, [3]Department of Atmospheric, Oceanic, and Space Sciences, University of Michigan, Ann Arbor, Michigan, USA, [4]Pisgah Astronomical Research Institute, Rosman, North Carolina, USA, [5]Department of Physics and Astronomy, Eastern Kentucky University, Richmond, Kentucky, USA, [6]Bradley Department of Electrical and Computer Engineering, Virginia Tech, Blacksburg, Virginia, USA, [7]Geophysical Institute, University of Alaska Fairbanks, Fairbanks, Alaska, USA, [8]Center for Solar-Terrestrial Research, Department of Physics, New Jersey Institute of Technology, Newark, New Jersey, USA, [9]Scientific Solutions, Inc., Chemlsford, Massachusetts, USA, [10]Center for Space Physics, Boston University, Boston, Massachusetts, USA

Abstract Observations of thermospheric neutral winds and temperatures obtained during a geomagnetic storm on 2 October 2013 from a network of six Fabry-Perot interferometers (FPIs) deployed in the Midwest United States are presented. Coincident with the commencement of the storm, the apparent horizontal wind is observed to surge westward and southward (toward the equator). Simultaneous to this surge in the apparent horizontal winds, an apparent downward wind of approximately 100 m/s lasting for 6 h is observed. The apparent neutral temperature is observed to increase by approximately 400 K over all of the sites. Observations from an all-sky imaging system operated at the Millstone Hill observatory indicate the presence of a stable auroral red (SAR) arc and diffuse red aurora during this time. We suggest that the large sustained apparent downward winds arise from contamination of the spectral profile of the nominal thermospheric 630.0 nm emission by 630.0 nm emission from a different (nonthermospheric) source. Modeling demonstrates that the effect of an additional population of 630.0 nm photons, with a distinct velocity and temperature distribution, introduces an apparent Doppler shift when the combined emissions from the two sources are analyzed as a single population. Thus, the apparent Doppler shifts should not be interpreted as the bulk motion of the thermosphere, calling into question results from previous FPI studies of midlatitude storm time thermospheric winds. One possible source of contamination could be fast O related to the infusion of low-energy O^+ ions from the magnetosphere. The presence of low-energy O^+ is supported by observations made by the Helium, Oxygen, Proton, and Electron spectrometer instruments on the twin Van Allen Probes spacecraft, which show an influx of low-energy ions during this period. These results emphasize the importance of distributed networks of instruments in understanding the complex dynamics that occur in the upper atmosphere during disturbed conditions.

1. Introduction

The thermospheric neutral wind plays an important role within the ionosphere-thermosphere-magnetosphere system, affecting the energy balance and composition of the upper atmosphere as well as generating electric fields and plasma instabilities. During geomagnetic storms, compression of the Earth's magnetosphere caused by the action of the enhanced solar wind develops intense electric fields that are mapped along geomagnetic field lines into the high-latitude ionosphere. Through collisions, $\mathbf{E} \times \mathbf{B}$ convection of plasma will drive the neutral winds sunward in the auroral region and antisunward within the polar cap. This convective behavior is governed in part by the sign of the interplanetary magnetic field which, if negative (southward), signifies the development of a two-cell convection pattern and, if positive (northward), causes the distortion of this two-cell pattern into a somewhat chaotic two- or multiple-cell pattern. At the same time, increased precipitation of energetic particles into the lower thermosphere altitudes appears with a concurrent equatorward expansion of the auroral zone and a large increase in ionospheric

conductivities. Coupling of the ionosphere-thermosphere system to the magnetosphere takes place with intense Birkeland currents flowing along geomagnetic field lines. The enhanced energy input into the polar region from these sources causes considerable heating of the ionized and neutral gases. The resulting uneven expansion of the thermosphere produces an equatorward pressure gradient force, driving strong neutral winds. The aeronomy literature is especially extensive regarding the subject of the ionospheric effects associated with geomagnetic storms [e.g., *Gonzalez et al.*, 1994; *Fuller-Rowell et al.*, 1997; *Prölss*, 1997; *Buonsanto*, 1999].

The disturbed polar thermospheric circulation alters the neutral composition and, at midlatitudes, moves the plasma up and down magnetic field lines, changing rates of production and recombination of the ionized species. At the same time the disturbed neutral winds produce polarization electric fields through a dynamo effect, as the neutrals collide with the plasma in the presence of the Earth's geomagnetic field. These electric fields affect the plasma, illustrating that the ionized and neutral species in the upper atmosphere are closely coupled, so it is not possible to gain a physical understanding of geomagnetic storm effects on ionospheric electron density without considering effects on the neutral thermosphere.

Beginning with *Hays and Roble* [1971], ground-based Fabry-Perot interferometer (FPI) observations during geomagnetic storm disturbances have consistently presented evidence showing increased meridional wind transport of heated air from the polar region to midlatitudes [e.g., *Hernandez and Roble*, 1976; *Sipler and Biondi*, 1979; *Hernandez and Roble*, 1984]. These results show large increases in the thermospheric temperatures and enhanced meridional winds to values as large as 500 m/s with large southward gradients in the meridional direction. *Meriwether* [2008] reviewed the modifications of low-latitude and midlatitude thermospheric dynamics that have been found to be associated with these disturbances.

In general, the horizontal component of the thermospheric wind field is 1 to 2 orders of magnitude greater than the vertical component. Assuming that the thermosphere is incompressible and in hydrostatic equilibrium, the vertical wind must be commensurate with the divergence in the horizontal wind, as derived in classical texts [*Holton*, 1972] or for the thermosphere by *Burnside et al.* [1981]:

$$w = H\left(\frac{\partial u}{\partial x} + \frac{\partial v}{\partial y}\right) \tag{1}$$

where the vector (x, y, z) is (east, north, up), the vector wind, (u, v, w), is in the same coordinates, and H is the scale height, around 50 km in the upper thermosphere. For typical horizontal scale sizes of the horizontal flow, and on time scales of hours, the magnitude of the vertical wind is not expected to be more than a few m/s [*Rishbeth et al.*, 1987; *Smith*, 1998]. However, measurements of persistent large vertical wind are not uncommon, especially at high latitudes [*Larsen and Meriwether*, 2012; *Nicolls et al.*, 2012]. *Spencer et al.* [1976] first observed large, 80 m/s vertical winds at the AE-C satellite, and ground-based instruments have measured vertical winds at auroral latitudes of a few tens of m/s [*Rees et al.*, 1984; *Ishii et al.*, 2001; *Smith*, 1998; *Nicolls et al.*, 2012; *Anderson et al.*, 2012; *Larsen and Meriwether*, 2012, and references therein]. *Anderson et al.* [2011] attempted to verify the Burnside relation using two spatially separated Fabry-Perot interferometers (FPIs) in Alaska to estimate the vertical wind and horizontal divergence. They found that equation (1) correctly estimates the sign of w on average, but that w varies significantly and is 3–4 times larger on average. *Smith and Hernandez* [1995] found that the Burnside relation can predict the wrong sign for the measured w.

The midlatitude thermosphere is typically more quiescent than the polar thermosphere, yet large apparent vertical winds are evident, particularly during periods of enhanced geomagnetic activity. *Hernandez* [1982] reported the vertical wind signature of a possible gravity wave with vertical motions as large as 25 m/s. *Sipler et al.* [1995] observed 50 m/s upward and downward winds during geomagnetically quiet times and a sustained 75 m/s downward wind for 2 h after the onset of a geomagnetic storm ($Kp = 8$), followed by a downward surge lasting 30 min, with peak downward flow of about 125 m/s. Other examples of midlatitude vertical wind measurements can be found in *Larsen and Meriwether* [2012], among others.

In this paper, we report observations made by the FPIs in NATION, the North American Thermosphere-Ionosphere Observing Network. Additional observations by an FPI and all-sky imager operated at the Millstone Hill Observatory as well as the Helium, Oxygen, Proton, and Electron spectrometer instruments on the twin Van Allen Probes spacecraft are presented. The observations were made during the geomagnetic storm of 2 October 2013 in which large increases in thermospheric wind speeds as well as gradients in the winds are seen across the effective field of view of NATION, consistent with previous single-site ground-based FPI

Table 1. Site Details for Locations of FPIs Used in This Study

Site	Latitude (°N)	Longitude (°E)
Millstone Hill, Massachusetts (MH)	42.61	288.52
Peach Mountain, Michigan (ANN)	42.27	276.25
Urbana Atmospheric Observatory, Illinois (UAO)	40.13	271.80
Eastern Kentucky University, Kentucky (EKU)	37.75	275.71
Virginia Tech, Virginia (VTI)	37.21	279.58
Pisgah Astronomical Research Institute, North Carolina (PAR)	35.20	277.15

studies of storm time thermosphere neutral winds. However, large apparent downward winds greater than 100 m/s are also seen in the observations, sustained over 6 h at all sites. We discuss the possibility that these apparent downward winds may not be indicative of bulk downward flow of the thermosphere but could be, at least partially, caused by contamination from an alternative source of the 630.0 nm emission during the ongoing geomagnetic storm.

2. Instrumentation

The North American Thermosphere-Ionosphere Observing Network (NATION) comprises five Fabry-Perot interferometer (FPI) sites in the midwestern portion of the United States, as detailed in Table 1. At each of the five sites, a CCD-based imaging FPI has been installed to observe the thermospheric redline emission at 630.0 nm. Under typical nighttime conditions, this emission is caused by the dissociative recombination of O_2^+ [*Link and Cogger*, 1988] which typically peaks at an altitude of approximately 250 km. Thus, the Doppler shift and Doppler broadening of the line measured by the FPIs is interpreted to correspond to the thermospheric winds and temperatures, respectively. The emission from a given look direction, selected by a dual-mirror SkyScanner system, is observed through an etalon, which sets up the circular interference pattern at the CCD. Each NATION etalon has a gap of 1.5 cm. The clear aperture of the FPIs is either 7.0 cm (Eastern Kentucky University (EKU), ANN, and Virginia Tech (VTI)) or 10.0 cm (Pisgah Astronomical Research Institute (PAR) and Urbana Atmospheric Observatory (UAO)). A frequency-stabilized HeNe laser provides the ability to determine the instrument function as well as providing a time-dependent Doppler reference for the wind estimates. Cloud monitors at each site, except the most recently installed site at Virginia Tech, are used to determine the viewing conditions at each site. Details of the network and instruments are described in *Makela et al.* [2012].

Three recent upgrades to the network have been made, yielding an improved ability to study the spatial and temporal dynamics of the thermosphere using NATION. First is the deployment of the fifth instrument from the New Jersey Institute of Technology, currently operated by and at Virginia Tech (VTI), expanding the longitudinal coverage of the network and providing additional bistatic and tristatic common volume measurement capabilities with the sites at Eastern Kentucky University (EKU) and the Pisgah Astronomical Research Institute (PARI). Second, an Internet-based control algorithm has been developed which synchronizes the observations at the various sites taking into account local viewing conditions (e.g., cloud coverage). Finally, real-time analysis of the images from each site has been implemented, allowing the control algorithm to dynamically change the integration times at each site to maintain a desired uncertainty in the resultant estimates of the thermospheric neutral winds and temperatures. These upgrades have improved the temporal resolution of the data from NATION without compromising the quality of the resultant parameter estimates.

Data are analyzed using the technique described in *Harding et al.* [2014]. In brief, the airglow interferograms are reduced to one-dimensional fringe patterns by an annular summation around the fringe center. This one-dimensional fringe pattern represents the convolution of the sky spectrum with the instrument function. A model of the instrument function that accounts for optical defects is fitted to the laser fringes, which are obtained by observing the frequency-stabilized HeNe laser. The parameters extracted from this model fit are used to fit a Gaussian spectral profile to the sky 630.0 nm airglow fringe, resulting in the Doppler shift and Doppler width estimates, assumed to be representative of the line-of-sight neutral wind and neutral temperature at 250 km.

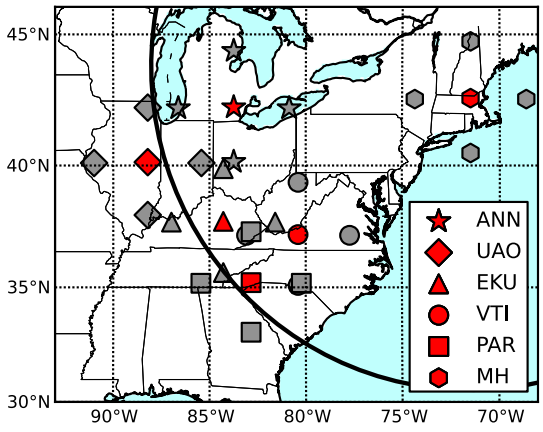

Figure 1. (Red markers) Locations of the five sites in the North American Thermosphere-Ionosphere Observing Network (NATION) and the Millstone Hill FPI. (Red and gray markers) Locations of thermospheric observations, assuming an emission altitude of 250 km. (Black arc) The edge of the field of view of the all-sky imager at Millstone Hill, assuming a minimum elevation angle of 10° and an emission altitude of 400 km (typical for the SAR arc presented in Figure 5).

A difficulty in FPI observations is establishing the zero reference, as the FPI is only able to specify the line-of-sight wind up to a constant offset. Although the laser observations provide a measure of the thermal variation of the zero reference over the night, they do not provide the absolute zero reference. This is because the wavelengths of both the HeNe laser and the red line O(^1D) emissions are not adequately known to allow the determination of the difference between the two wavelengths with the necessary accuracy to measure vertical winds in an absolute sense with an error of less than a few m/s. Typically, the absolute zero reference is established by assuming that while the instantaneous vertical wind may not be zero, the averaged vertical wind over the night, computed from all zenith observations, is zero. For nights with large sustained apparent vertical winds, such as the one presented in this paper, this assumption is invalid. Thus, for this paper, it is assumed that the vertical wind averaged over the prestorm period (00–02 UT) is zero and that instrument performance does not vary from the prestorm characteristics over the time frame of the storm. At one site (ANN), the laser frequency stabilization failed, as evidenced by the linear drift in the estimated etalon gap and by the drift in the laser intensity (not shown), which is used as a proxy for the laser wavelength in the stabilizer control loop. If this laser wavelength drift is not corrected, a linear drift of 50 m/s over the night is seen superimposed on the vertical wind estimate. For this site only, this drift is removed by assuming the poststorm vertical winds (09–12 UT) are also zero and the laser wavelength varies linearly with time.

An additional FPI, operated at the Millstone Hill Observatory (MH in Table 1 and Figure 1), made observations of the 630.0 nm emission on this night. The MH FPI has a clear aperture of 12 cm and gap of 1.0525 cm. Five orders of the interference pattern are analyzed by fitting the annular integrated fringes to a Gaussian in order to produce estimates of the Doppler shift and broadening effects [*Kerr*, 2014]. The wind errors are on the order of 1–2 m/s, which is dependent on the airglow intensity. Observations of a frequency-stabilized HeNe laser are used to monitor the instrument drift and provide a zero Doppler reference, as is done for the NATION FPIs.

3. Observations

The five NATION FPIs were operating on the night of 1–2 October 2013. The first observations were obtained at the VTI instrument on 1 October 2013 at 2341 UT, continuing until the last observation made by the UAO instrument on 2 October 2013 at 1111 UT (UT is 4 h ahead of LT for the sites at VTI, PAR, EKU, and ANN and is 5 h ahead of LT at UAO. All sites were observing daylight savings time during this period). All five instruments were collecting data between 0013 and 1040 UT on 2 October 2013. Viewing conditions, as determined by the cloud sensor installed at the sites, were very good with brief periods of clouds concentrated shortly after local sunset at PAR (00–02 UT) and before sunrise at EKU (10–11 UT) and UAO (09–11 UT). ANN experienced two brief (30 min) periods of cloud coverage between 08 and 10 UT. Although no cloud sensor was installed at the VTI site at that time, the local weather reports [*weatherunderground.com*, 2013] indicated clear viewing conditions until 0730 UT, which is borne out by the quality of the observations obtained from that site.

The instruments were configured in a mode that emphasized the cardinal observing directions with a laser calibration image obtained for determining the instrument function and drift every ~20 min. The location of each observing direction, assuming an emission altitude of 250 km, is shown in Figure 1. The NATION observations cover over 10° in both latitude and longitude. Integration times for the laser images were fixed at 30 s, while integration times for the sky images were allowed to vary between 30 and 300 s per image.

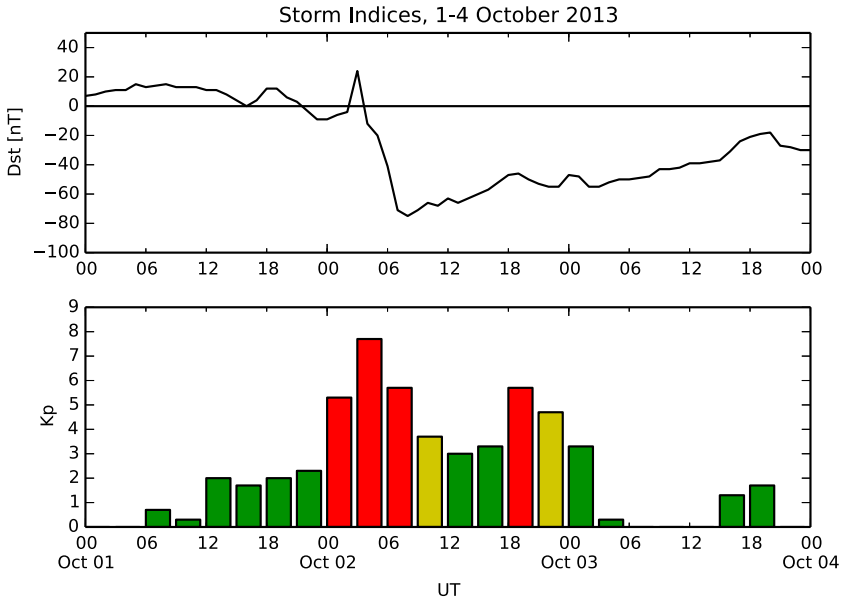

Figure 2. (top) *Dst* and (bottom) *Kp* indices for the period of 1–4 October 2013.

These constraints allowed the control program to maintain a signal-to-noise ratio for the collected interferograms sufficient to yield uncertainties below 5 m/s (line-of-sight velocity) and 20 K (temperature) at each site.

The Millstone Hill FPI made observations of the 630.0 nm emission beginning at 2304 UT on 01 October 2013 and ending at 0959 UT on 02 October 2013. No sky images were obtained from approximately 04 to 05 UT, due to the instrument taking a series of flat field images used in the analysis. The instrument uses a 45° elevation angle at four cardinal directions and zenith with an integration time of 3 min. Observations of the laser are made approximately once every hour. Cloud coverage, as indicated by a collocated all-sky imager (see below), was negligible on this night.

A filament eruption occurred on the Sun on 29 September 2013. Early on 2 October 2013, the associated coronal mass ejection passed the ACE satellite, which measured a rapid increase of solar wind velocity to 600 km/s and a strong southward interplanetary magnetic field of 30 nT [*Space Weather Prediction Center*, 2013]. The prevailing geophysical conditions during this event, as captured by the *Dst* and *Kp* indices are presented in Figure 2. *Dst* increased from a slightly positive value to 24 nT at 03 UT on 2 October 2013 before decreasing and eventually reaching −75 nT at 8 UT on 2 October 2013. The *Kp* index increased to a value of 5^+ between 00 and 03 UT, rose to 8^- between 03 and 06 UT, and reduced to 6^- and then 4^- from 06 to 12 UT. Thus, the observations presented here from the NATION FPIs cover the onset of a storm period as observed from the local premidnight sector.

Measurements of the Doppler shift of the 630.0 nm emission in the vertical direction are obtained by observations looking toward zenith at each site. The vertical winds deduced from these observations made by the NATION and MH FPIs on this night are shown in Figure 3 (top). In this figure, a stack plot of the temporal variations of the apparent vertical wind for all five sites is presented, with the *y* offset for each measurement representing the latitude corresponding to the observations. Observations made from the NATION FPIs over the past year indicate that typical quiet time values of vertical winds are quite small: less than 10 m/s. However, on this night, the observations suggest strong downward winds at all sites, beginning at roughly 0300 UT. Apparent downward winds of 150 m/s are observed over ANN, with weaker winds seen over the sites to the south, indicating a latitudinal gradient in the apparent downward winds. A strong downward pulse is seen over the NATION sites beginning at 0420 UT and lasting for approximately 40 min. The strength of the pulse is seen to be a strong function of latitude (−300 m/s at ANN and −130 m/s at PAR). The apparent downwelling gradually subsides, returning to values close to 0 m/s, with the southernmost reaching zero before the northern sites (0800 UT at PAR and 0845 UT at ANN). No data from MH is available at this time due to the instrument taking flat field images from approximately 04 to 05 UT.

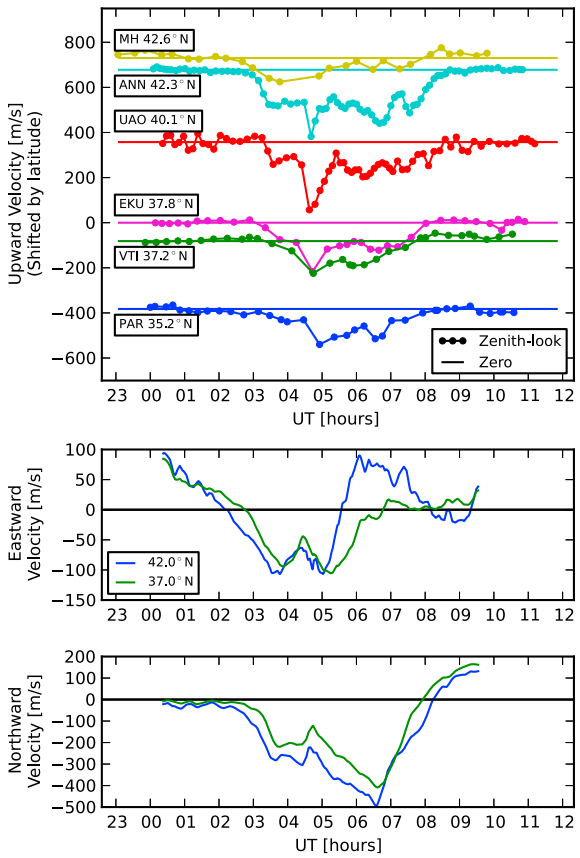

Figure 3. (top) Estimates of apparent vertical winds made by FPIs at each NATION site and MH. A *y* offset for each site has been applied proportional to the latitude of each site. (middle) Zonal and (bottom) meridional winds derived from the field-fitting procedure described in the text. Winds at locations representative of the (blue) northern-central and (green) southern-central regions of the NATION field of view are presented. The average statistical uncertainty of the estimated wind measurements is less than 5 m/s.

The analysis of the horizontal wind presents more challenges than the vertical wind. The observations are made at a 45° zenith angle, so the measured line-of-sight velocity represents a combination of the horizontal wind and the vertical wind. On quiet days, the horizontal contribution to the line-of-sight wind is extracted by assuming that the vertical wind field is locally uniform and applying the vertical wind measured in the zenith direction above each site to the oblique measurement, although the two measurement locations in the thermosphere are separated by 250 km. On this night the apparent vertical wind field is not uniform, so this technique would introduce large errors into the estimates of the horizontal winds.

Instead of attempting to estimate the horizontal wind from each line-of-sight measurement, the apparent wind field over the NATION array is estimated directly from the set of all instruments' raw line-of-sight measurements, assuming that the wind field, (u, v, w), can be approximated by a low-order polynomial in latitude and longitude. For this initial analysis, a linear approximation is used:

$$u = u_0 + u_1 y + u_2 x \tag{2}$$

where u_0, u_1, and u_2 are unknown coefficients to be estimated, x is east-west distance, and y is north-south distance. Analogous equations for v and w are also used. Combining the expressions for all line-of-sight winds results in a matrix equation, which can be inverted in a least-squares sense to obtain the nine unknowns. This provides a linear approximation to the wind field that represents the large-scale flow implied by the data, but does not capture small-scale spatial structure. It is found that the data are reasonably well represented by the large-scale flow, as the residual between the data and linear fit is 28 m/s RMS (root-mean-squared) over the night. We solve for the temporal variation of this wind field fit at a 60 s cadence. Since the line-of-sight measurements at the different locations are taken at different times, the velocities used in the inversion are linearly interpolated in time. Animations of the wind field derived in this way are presented in the supporting information for this paper.

The apparent horizontal neutral winds estimated by the technique above are shown in Figure 3 (middle and bottom). The results of the inversion (see Animation S1) indicate that the longitudinal gradients (e.g., u_2) are often much smaller than the latitudinal gradients (e.g., u_1). Thus, we present the apparent horizontal wind field evaluated at two locations separated by 5° in latitude: (42°N, 83.9°W) and (37°N, 83.9°W), which are representative of the northern-central and southern-central regions of the NATION field of view. Strong equatorward winds (indicated by the negative sign in the meridional winds presented in Figure 3 (bottom)) are observed at the northern latitudes beginning at approximately 0230 UT. At this time, the typically equatorward winds of $\sim$ 25 m/s are seen to dramatically increase to 300 m/s at around 0330 UT, eventually reaching 450 m/s by 0630 UT. This increase in equatorward wind is observed at the southern latitudes as well, but with smaller magnitudes, indicating that the NATION network is observing the effects of the geomagnetic storm impinging from higher latitudes. This chain of events in the meridional winds fits

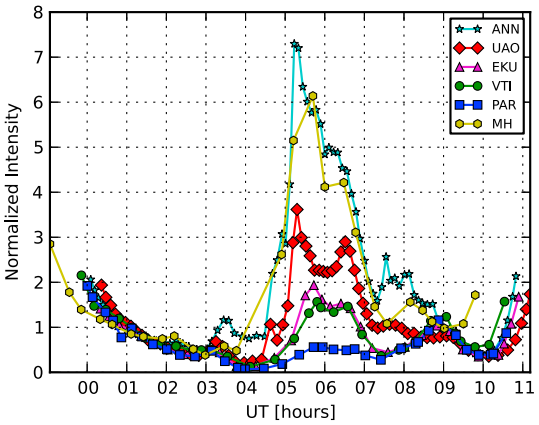

Figure 4. Zenith airglow intensities measured by each of the NATION FPIs. The uncalibrated intensities have been normalized to each other over the period of 01–02 UT.

well with observations from previous storms, including in situ observations [e.g., *Earle et al.*, 2013]. The equatorward winds gradually subside before turning poleward around 0800 UT. Thus, the strong equatorward winds of greater than 200 m/s are observed to persist for at least 4 h across the NATION field of view.

Concurrent to the initial surge in the equatorward winds at the onset of the storm, the zonal winds (positive eastward, Figure 3 (middle)) are seen to decrease from their typical eastward values early in the night, reversing to a westward wind of approximately 75 m/s by 04 UT. Westward turning of the winds is consistent with the Coriolis force acting on the southward flowing storm-induced winds and is commonly observed during storm conditions.

Concurrent to the strong downward pulse in the apparent vertical wind from about 0420–0500 UT is a pulse in the apparent zonal and meridional winds. The eastward and northward pulse is seen superposed on the large westward and southward surge and has a magnitude of approximately 100 m/s and 50 m/s in the zonal and meridional directions, respectively.

The relative, normalized airglow intensity measured in the zenith direction at each site is shown in Figure 4. The various FPIs have been calibrated relative to each other by assuming that during 01–02 UT they observe the same mean intensity. Absolute calibration is unknown, so it is shown on an arbitrary scale.

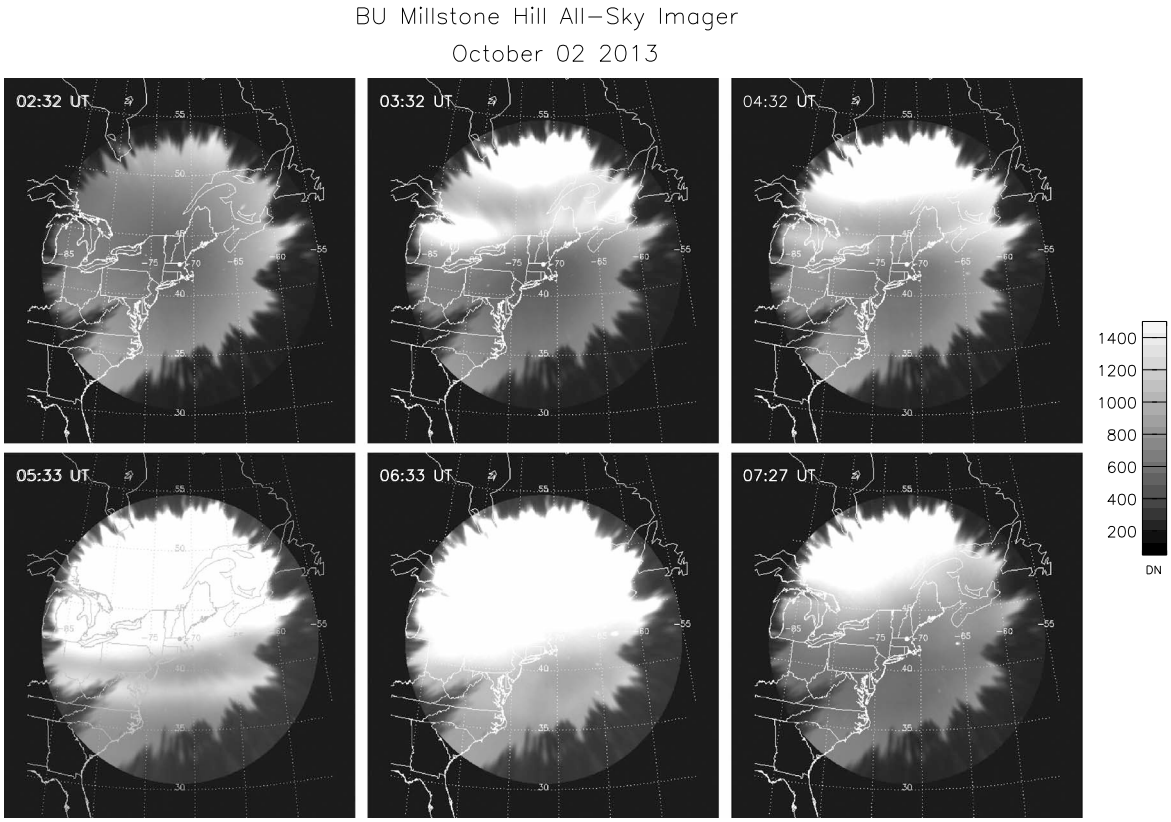

Figure 5. All-sky images of the 630.0 nm emission, projected onto a map assuming a 400 km altitude layer. One image per hour between 0230 and 0730 UT is presented.

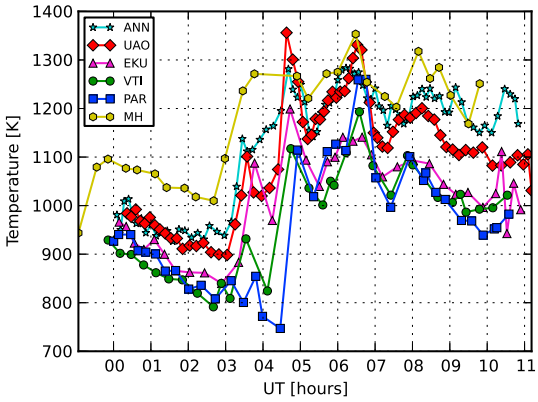

Figure 6. Thermospheric temperatures estimated in the zenith direction by each of the NATION FPIs. The average statistical uncertainty is 16 K.

At 0300 UT, coincident with the arrival of the southward and downward wind, an intensity increase by a factor of 2 is seen in the northernmost site (ANN), while a more modest increase is seen in the southern sites, indicating a northward gradient in intensity that persists until about 0830 UT. Beginning at 0430 UT, coincident with the arrival of the large −150 m/s apparent vertical wind, a large increase in the intensity commences. It grows fastest and largest at the northern sites, by a factor of about 5. The intensity remains high until the large southward and downward surge abates around 0700–0800 UT. Beginning around 0800 UT, and concurrent with the arrival of the northward meridional wind, a weaker intensity increase is seen in the southern sites (PAR, VTI, and EKU), which briefly reverses the gradient in intensity.

To give a broader context to the intensity variations and further indication of the disturbed nature of the midlatitude ionosphere, we present imaging data obtained from the Boston University all-sky imager collocated with the MH FPI. A sample of images obtained at 630.0 nm between 0230 and 0730 UT are shown in Figure 5. Observations above 10° elevation are mapped upon a geographic grid assuming an emission height of 400 km and provide a 160° field of view. The center of each image corresponds to the zenith direction. The full field of view is blocked by trees for low-elevation angles. Diffuse aurora is seen in the images coincident with the increase in the observed intensity from the FPIs shown in Figure 4. A stable auroral red (SAR) arc is seen in the images between 0330 and 0530 UT, propagating over the NATION FPIs between approximately 0430 and 0530 UT, coincident with the large pulse seen in the apparent vertical winds. The SAR arc reaches equatorward of 35°N.

The apparent thermospheric temperature measured in the zenith direction at each site is shown in Figure 6. At the beginning of the night, the temperature follows its typical pattern of cooling until 0300 UT, at which time a temperature increase is seen over both ANN and MH, with increases seen later over the more southern sites. The apparent temperature peaks around 0430 UT, coincident with the large downward pulse seen in the wind. Another peak is seen around 0630 UT, associated with the maximum southward wind (see Figure 3). A third minor peak is seen around 0800 UT over the southern sites, coincident with the reversal of the meridional wind.

An unusual feature of the temperature measurement is its apparent anisotropy. In Figure 7 the temperature measurements looking south from ANN and north from EKU are compared. Both measurements are made at a zenith angle of 45°. At the assumed emission altitude of 250 km, these measurement locations differ by 54 km horizontally. On a typical quiet night, these measurements agree to within a couple tens of Kelvin. However, on this night, there is a clear systematic difference, with the south-looking measurement exceeding the north-looking measurement by an average of 93 K during the storm period. Similar results hold for the three other common measurement locations in the NATION network: the south-looking temperature measurement exceeds the other measurements in a systematic and statistically significant way (not shown). Since the south-looking direction is approximately antiparallel to the magnetic field, these results indicate that the velocity of the emitting species, atomic oxygen, is not isotropic: its velocity distribution is wider along

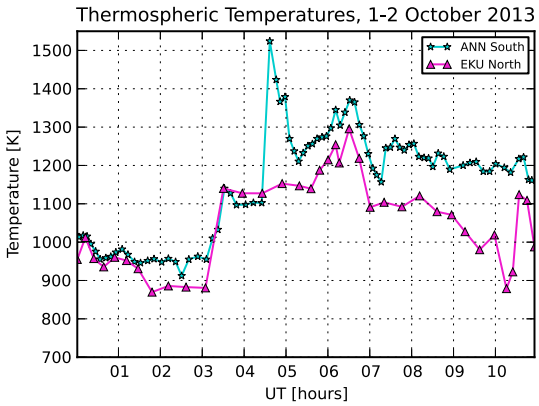

Figure 7. Comparison of the thermospheric temperatures observed looking to the south from ANN and to the north from EKU. The thermospheric pierce points at 250 km for these two observations are separated by 54 km.

the magnetic field than perpendicular to it. This anisotropy in the velocity distribution is consistent with the effect of energetic O^+ streaming down the magnetic field line, a possibility discussed in more detail in the next section.

4. Discussion

The FPI observations presented in the previous section, as well as the corresponding *Dst* (ring current) and *Kp* (geomagnetic) indices, clearly indicate that the midlatitude thermosphere is experiencing storm conditions. Many of the features of the estimated neutral winds and temperatures are consistent with previous studies of the midlatitude thermosphere during similar conditions. For example, the increase in the equatorward winds, the reversal of the zonal flow from eastward to westward, as well as the increase in thermospheric temperatures indicated in Figures 3 and 6 match well with current understanding of the thermosphere's response to increased high-latitude heating [e.g., *Rishbeth et al.*, 1987]. Similarly, the existence of vertical winds in the thermosphere associated with large-scale circulation patterns generated by heating in the auroral region have been observed previously [e.g., *Rishbeth et al.*, 1987; *Sipler et al.*, 1995; *Larsen and Meriwether*, 2012]. However, downwelling over such a large spatial region (20° in longitude and 10° in latitude) with the magnitude (100 m/s) and duration (6 h) indicated by the observations presented above is difficult to explain, as is the temperature anisotropy observed when viewing the same thermospheric volume from different look directions. These anomalous observations, consistent across all of the FPIs in NATION, indicate that the 630.0 nm emission at midlatitudes during storm conditions is most likely not representative of bulk flow of the thermospheric neutrals.

We first examine whether the apparent downward wind presented in Figure 3 could be an instrumental artifact. The method utilized to deduce the vertical wind assumes that the frequency-stabilized laser is, in fact, stable over time and that the vertical winds are zero on average during the period used to set the zero reference. As to the first assumption, it is true that any drift or temporal changes in the laser frequency would manifest as temporally varying apparent vertical wind. However, it is extremely unlikely that the lasers operated at the five independent sites would show the same temporal properties as to give rise to the similar patterns seen in the apparent vertical winds seen in Figure 3 and that a clear latitudinal dependence on the magnitude of the apparent vertical winds would be seen. As to the second assumption, if the actual vertical winds during the period used to set the zero reference were nonzero on average, this would manifest as a constant bias in the apparent vertical winds and, again, could not explain the temporal properties evident in the vertical winds presented in Figure 3. In addition, the fact that the apparent vertical winds are observed by the MH FPI, which uses a different etalon gap than the NATION FPIs and employs a different analysis technique, indicates that the effect is not confined to the specific design of the NATION FPIs. Thus, we are confident that the observations presented in this figure cannot be instrumental artifacts or by-products of the assumptions used in deriving the zero Doppler reference.

The Burnside relation (1) can be exercised to examine whether the horizontal neutral winds are consistent with the vertical winds estimated from the zenith observations. This is possible given the spatially distributed observations provided by the FPIs in NATION combined with the field-fitting procedure described above. In both the raw measurements and the results of the field fitting, divergence in the horizontal flow is evident, which should be associated with vertical flow. In Figure 8, the vertical winds obtained from the field fit are compared with those expected from the observed divergence in the horizontal winds at the center of the NATION field of view, assuming a scale height of 50 km. The magnitude of the Burnside vertical wind is seen to vary between −15 and 5 m/s over the course of the night. It is significantly smaller in magnitude than the vertical winds estimated from the zenith look directions and occasionally disagrees in sign. Such a discrepancy has been observed before [*Smith and Hernandez*, 1995].

Of course, the assumptions used in deriving (1) (most notably, hydrostatic equilibrium and the neutral scale height) might become invalid during storm conditions, calling into question the applicability of the Burnside relation to the observations presented here. Indeed, modeling studies indicate that relaxing the hydrostatic assumption results in larger vertical winds in the thermosphere [*Yigit et al.*, 2012]. However, these studies do not indicate sustained downward winds of the duration and magnitude presented here. In fact, *Deng et al.* [2008] showed that when a strong, sustained energy input into the thermosphere is present, there is rapid imbalance in the pressure gradient and gravity, which causes an upward velocity. The imbalance is rapidly reduced, and the velocity decreases slowly over a few tens of minutes. The hydrostatic balance

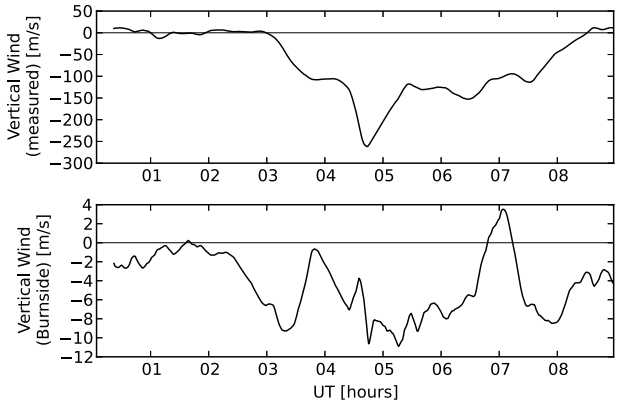

Figure 8. (top) Apparent vertical wind calculated from the field-fitting procedure and (bottom) vertical wind due to the divergence in the horizontal wind field over the center of the NATION field of view calculated using the Burnside relation.

is only broken for a few minutes, which means that the Burnside relation should be applicable on time scales longer than several minutes.

In considering possible alternative explanations for the development of these surprising apparent downward vertical wind speeds observed, the possibility of contamination of the observed 630.0 nm spectral profile, suggested by *Hampton et al.* [2012] in the context of auroral vertical winds, emerges as a possible explanation. The precipitation of energetic O^+ ions has previously been observed at 800 km over the energy range of 0.7 to 12 keV during periods of geomagnetic storm activity [*Shelley et al.*, 1972; *Sharp et al.*, 1976a, 1976b]. Charge exchange of these energetic O^+ ions with neutrals as well as the momentum exchange resulting from the elastic scattering of precipitating ions with O would both produce fast O atoms [*Torr et al.*, 1974, 1982]. Thermalization of these atoms by quenching processes would occur at different rates depending upon the ion deposition altitude. However, *Ishimoto et al.* [1994] presented model calculations indicating that the collisional interactions of these fast O atoms with the ambient atoms would generate a population of 630.0 nm photons with an overall Doppler shift ranging from 1 to 15 pm (500 to 7000 m/s). *Torr et al.* [1974] estimated that the fast O population could create excitation of 630.0 nm emission of as much as 200 R.

The work of *Torr et al.* [1974], *Torr and Torr* [1979], and *Torr et al.* [1982] suggests that much of the population of fast O atoms would be moving upward. However, to produce an apparent downward wind, much of the fast O atoms would need to be moving in the downward direction. The partition of the incoming ion flux into downstream and upstream populations of fast O atoms with energies of 20 to 1000 eV was computed by *Ishimoto et al.* [1992], showing that the downstream populations were significantly larger than the upstream population at the three altitudes of 242 km, 283 km, and 370 km.

Indication of an injection of low-energy O^+ ions into the inner magnetosphere and ring current during the 2 October 2013 storm period considered here is provided by the Energetic Particle, Composition, and Thermal Plasma Suite's (ECT) Helium, Oxygen, Proton, and Electron (HOPE) mass spectrometer instruments on the twin Van Allen Probes spacecraft [*Funsten et al.*, 2013]. Results from these instruments are shown in Figure 9, indicating that O^+, as well as other ionic species, is readily available in the inner magnetosphere. This O^+ population originates from polar up-flow sources and is transported into the inner magnetosphere and ring current from the tail via a combination of both steady cross-tail and impulsive electric fields as well as resonant wave interactions [e.g., *Welling and Ridley*, 2010; *Keika et al.*, 2013, and references therein]. Coincident with the period of apparent downward winds observed by the NATION FPIs is an infusion of low-energy ion species, including O^+. An especially strong increase in the flux is seen at the same time as the largest apparent downward winds (04–05 UT). Although the northern magnetic footprints for the two spacecraft, near Alaska, were to the west and north of the region of the thermosphere observed by NATION, it would be expected that the influx of low-energy O^+ took place over the nightside auroral and subauroral region, which sweeps geographically down in latitude over the midlatitudes observed by NATION.

The O^+ present in the inner magnetosphere can be lost via a number of mechanisms (e.g., radial diffusion, charge exchange, coulomb collision, pitch angle scattering) [*Daglis et al.*, 1999]. Pitch angle scattering would cause O^+ to stream down field lines into the loss cone. These O^+ ions would collide with the neutral O, resulting in the production of fast O, both at the spacecraft footprints and more geographically extended regions, depending on magnetospheric processes driving the O^+ precipitation and atmospheric density. These fast neutral atoms gradually become partially thermalized through quenching processes and redistributed across the midlatitude region. As indicated by the *Ishimoto et al.* [1994] analysis, these processes

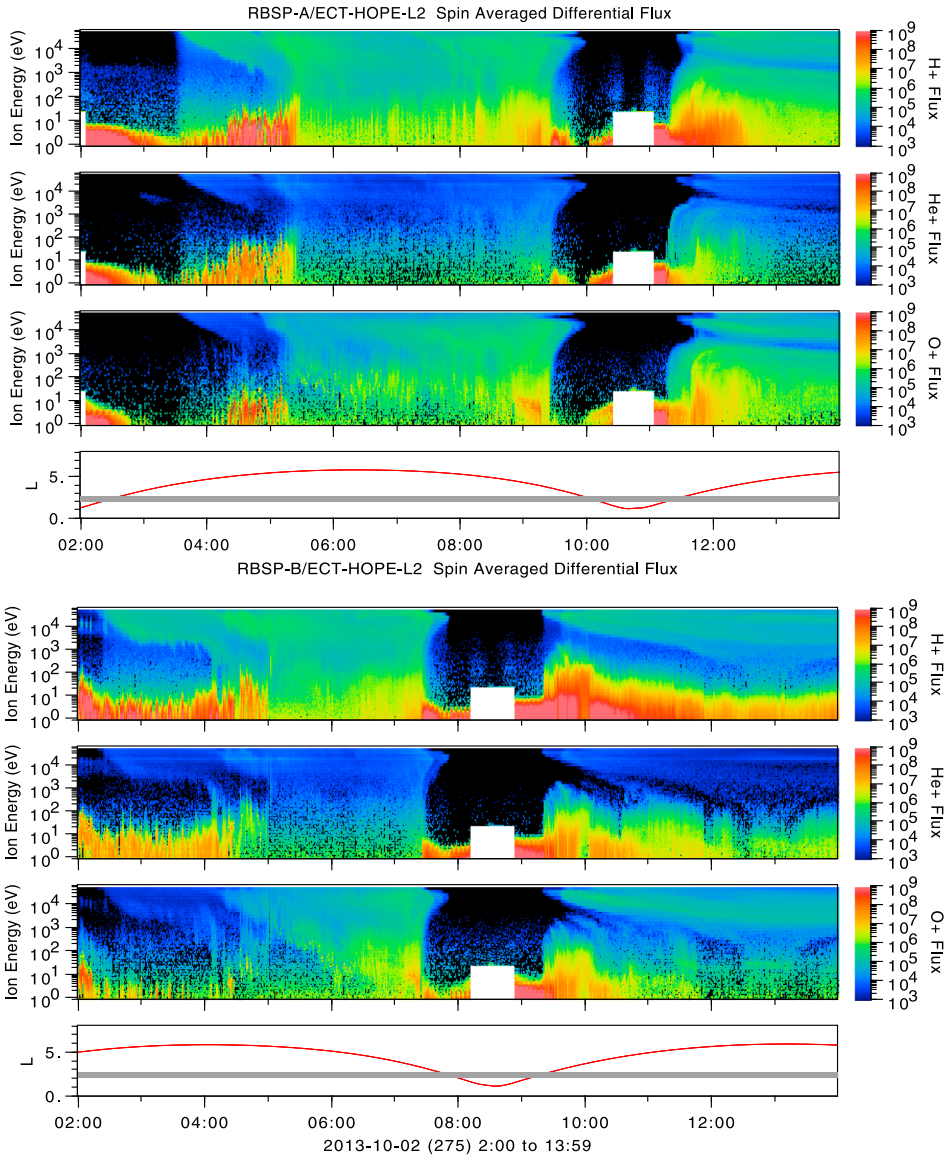

Figure 9. ECT-HOPE data for H^+, He^+, and O^+ differential flux (particles/(s·cm^2·keV·str)) from Van Allen Probes spacecraft (top) A and (bottom) B for 2 October 2013. The panel at the bottom in Figures 9 (top) and 9 (bottom) shows (red line) the *L* shell from which the satellite observations come from as well as (gray line) the approximate *L* shell corresponding to the ground-based FPI observations.

would result in an emission at 630.0 nm sourced by nonthermospheric processes, with an appreciable Doppler shift. The contamination caused by this second population of 630.0 nm photons, with a velocity and thermal distribution different from the thermospheric population of 630.0 nm photons, could be responsible for the large apparent winds and anisotropic temperature estimates discussed above. This is because the analysis employed assumes a single population of 630.0 nm photons.

To test this explanation for the observed apparent downward wind, we present a simple model of fast O contamination of the 630.0 nm emission. The normal contribution to the emission, arising from the dissociative recombination of O_2^+, is modeled as a Gaussian with a 0 m/s Doppler shift and a temperature of 800 K. The effect of the fast O contamination is modeled by the addition of a second Gaussian with a specified apparent downward speed (ranging from 643 to 1000 m/s, in line with the lower speeds in the *Ishimoto et al.* [1994] study), intensity (referenced to the intensity of the nominal thermospheric dissociative recombination contribution), and temperature (taken to be 800 K). Three examples are presented in Figure 10, showing the apparent temperature and speed caused by analyzing the combined spectral profile as if it were a single

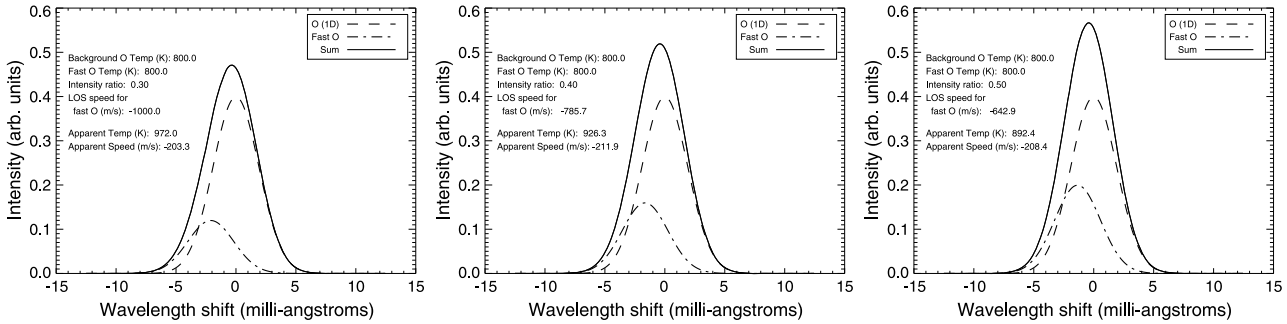

Figure 10. Three examples of the effect of fast O contamination on the apparent temperatures and Doppler velocities obtained by analyzing the 630.0 nm emission profile using a single Gaussian. In each panel, the modeled O(^1D) contribution (dashed), fast O (dash-dotted), and the total emission (solid) is presented. Parameters used in the model are presented in each panel.

Gaussian arising from dissociative recombination. Apparent speeds of −200 m/s with apparent temperature increases of more than 100 K are possible with reasonable speeds and intensity ratios for the fast O contamination. Fitting of the combined spectral profile using an Airy profile rather than a single Gaussian would produce similar results for the Doppler shift. A more thorough investigation of the parameter space is shown in Figure 11, showing the dependence of the effective speed on the intensity ratio between the nominal line and that due to the nonthermospheric contamination. This figure indicates that the spectral properties (e.g., intensity) of the emission line originating from the hypothesized fast O contamination will change the relationship between the speed and temperature of the fast O population, the speed and temperature of the nominal thermospheric population, and the effective speed obtained from fitting a single Gaussian to the combined spectral profile.

The resulting shower of fast O atoms can also be expected to produce heating of the atmosphere for the region above 200 km [*Torr et al.*, 1974; *Torr and Torr*, 1979; *Torr et al.*, 1982], which is consistent with the observed NATION increase of 350–400 K near 0430 UT. *Torr et al.* [1982] estimated that the peak heating rate due to large nocturnal energetic ion sources can be comparable to the dayside EUV source at high altitudes. Their analysis using the National Center for Atmospheric Research general circulation model found the storm temperature perturbation near 400 km at the time of maximum heating would be of the order of 400 K. However, it is important to point out that contamination of the spectral line shape due to the fast O atoms would result in an anomalous (nonphysical) temperature increase, as indicated in Figure 10. Given the limitations of our current measurements, it might be impossible to unravel these two competing effects without additional information. However, it is reasonable to conclude from Figure 7 that the nonphysical temperature increase is at least 100 K, because the velocity distribution along the field line is wider than the distribution across it, by an amount equivalent to a 100 K increase. This anisotropy could not result from a physical temperature increase.

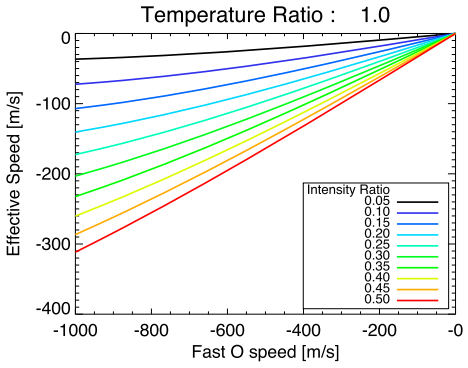

Figure 11. Effective speed as a function of the speed of fast O contamination (relative to the population of 630.0 nm photons arising from thermospheric sources) for a range of intensity ratios between the nominal 630.0 nm emission arising from dissociative recombination and that from the fast O contamination at a temperature ratio of 1.0.

Although the proposed contaminating population of 630.0 nm photons would cause an extra bump in the nominally Gaussian emission spectrum, no direct evidence of this contamination was found in the raw sky fringes. This is expected for two reasons. First, as seen in Figure 10, the speed of O, while large compared to the thermospheric wind, is small compared to the thermal spread of the nominal emission, and thus, the resulting composite spectral shape is difficult to distinguish from a true Gaussian. Second, the FPIs used in the NATION array have a relatively low finesse (15), related to the resolution of the system, so our

ability to resolve subtle spectral features is limited. If a more sophisticated analysis technique cannot separate the contributions from the two populations, the instruments may need to be redesigned to increase their resolving power in order to directly study the spectral shape and distinguish between the nominal 630.0 nm spectral profile caused by dissociative recombination and that due to the fast O. As shown above, the relative intensities and temperatures of the nominal 630.0 nm emission and that caused by the fast O contamination will determine the estimated velocities and temperatures.

It is important to point out that the contamination effect would be present in both the vertical and horizontal wind estimates. The apparent vertical winds are a combination of the actual vertical motion of the thermospheric neutrals as well as the projected vertical velocity of the fast O contamination. Even for the zenith look direction and assuming that the thermospheric population has zero vertical velocity, we cannot unambiguously estimate the primarily field-aligned contribution from the hypothesized contamination source. This is because we lack information on the relative intensity and temperature ratios of these two populations, which affect the overall estimated Doppler shift (see Figures 10 and 11). For example, the three cases presented in Figure 10 all result in an estimate of a approximately 200 m/s Doppler shift despite a Doppler shift for the contaminating population ranging from 640 to 1000 m/s. Thus, simply treating the apparent vertical wind as an actual vertical wind and removing it from the line-of-sight measurements made in the off-zenith directions is not a correct way for them to be handled. A more detailed analysis is needed to understand if reliable horizontal wind estimates can be obtained under these conditions.

Understanding the overall effect of this hypothesized contamination source upon the 630.0 nm spectral profile and the inferred winds and temperatures would require expanding on the work of *Ishimoto et al.* [1994], including the application of a model of the FPI instrument. A detailed modeling of the energy deposition of these energetic ions is needed to estimate the extent that this contamination would result in an apparent Doppler shift, but the simulation presented here indicates that this is a plausible explanation for the apparent downward winds observed by the NATION FPIs. This spectral contamination hypothesis would explain the latitudinal reduction of the apparent vertical wind seen by NATION as this effect is consistent with a similar latitudinal dependence of the energetic influx of these O^+ ions [*Sharp et al.*, 1976b].

It is relevant to note that previous studies have provided evidence of nonthermal oxygen atoms in the thermosphere, even during geomagnetically quiet periods. Such quiet time nonthermal oxygen atoms are thought to be produced mainly by dissociative recombination of O_2^+ and NO^+ [*Hickey et al.*, 1995], as opposed to charge exchange with precipitating O^+ during active times, as discussed in the present paper. Observational evidence of this nonthermal population utilizes various techniques: twilight observations of the 732.0 and 733.0 nm airglow emission from the ground [*Yee et al.*, 1980], redline intensity measurements made by the Visible Airglow Experiment on the Atmosphere Explorer-C satellite [*Schmitt et al.*, 1981], red line temperature measurements from the FPI on the Dynamics Explorer satellite [*Hubert et al.*, 2001], and in situ measurements made by the low energy neutral atom (LENA) instrument on the IMAGE spacecraft [*Wilson and Moore*, 2005]. This evidence is supported by modeling which suggests that a nonthermal population is present above 200 km, which should increase FPI red line temperature measurements above the ambient temperature [*Shematovich et al.*, 1999; *Sipler and Biondi*, 2003; *Kharchenko et al.*, 2005]. In this paper, we present observational evidence that nonthermal oxygen atoms affect the wind measurement as well as the temperature, at least during geomagnetically active periods.

5. Summary

In this study, observations obtained from a distributed network of six Fabry-Perot interferometers measuring the 630.0 nm emission, nominally caused by the dissociative recombination of O_2^+ and indicative of thermospheric winds have been presented. The results indicate that the midlatitude thermosphere over North America during the storm of 2 October 2013 was quite disturbed with estimated equatorward thermospheric winds reaching 300 m/s. Large vertical winds are observed from all of the sites, with estimated apparent downward winds of more than 100 m/s observed for 6 h during the storm.

This study explores the possibility that the large downward flows are not indicative of bulk flow of the thermosphere but, rather, are due to contamination of the 630.0 nm spectral profile by a population of fast O related to the infusion of low-energy O^+ ions, as observed by the ECT-HOPE instrument on the Van Allen Probes. The measurements indicate that such O^+ was readily available in the inner magnetosphere, originating from polar up-flow sources and transported into the inner magnetosphere and ring current via

dawn-to-dusk electric fields. Such O^+ can then be lost via a number of mechanisms, one of which is pitch angle scattering, which would cause the O^+ to precipitate into the thermosphere [*Daglis et al.*, 1999]. This would result in the production of fast O across the nightside auroral and subauroral regions. Ground-based all-sky observations indicate the simultaneous occurrence of diffuse aurora and a SAR arc.

Thus, we suggest that our results of anomalously large downward vertical winds, especially when viewed from the perspective of the *Ishimoto et al.* [1994] analysis, provide support for the identification of incoming energetic O^+ ions as an important component of geomagnetic storm activity at midlatitudes. These ions generate fast O through charge exchange and momentum transfer interactions. Preliminary modeling of the spectral contribution induced by a fast O population at 630.0 nm supports this explanation, which can account for the large apparent vertical winds as well as some of the temperature increases estimated from the FPI measurements. Although there is likely atmospheric heating occurring during the storm period, which would cause the atmosphere to move upward, in the current analysis of the FPI measurements alone, we cannot conclude how much of the apparent heating is due to actual atmospheric heating and how much is due to the hypothesized contamination.

The results of this study demonstrate the need to monitor the instrument drift through the use of a frequency-stabilized laser (or a similar reference source) and not make the assumption that the vertical wind is zero at all times, which historically has been a common assumption made in analyzing FPI data. Indeed, the results of analyzing the data using the zero vertical wind assumption (not shown) yield results that appear reasonable and are in line with previous midlatitude storm studies conducted from single sites. However, in this type of analysis, a few oddities result, such as apparent discrepancies between the meridional flow at common volume locations observed from different sites. These types of discrepancies would not have been noted from observations from a single site and so this type of contamination, and its effects on the estimated wind field, would have gone unnoticed. Therefore, the results of this study emphasize the necessity of distributed networks of instruments to understand the complex dynamics that occur in the thermosphere/ionosphere during disturbed conditions.

To determine if the hypothesized contamination of the FPI measurements by emissions due to fast O is correct, further investigations are needed to be able to decouple its effect on the measurements from the bulk thermospheric flow. For example, it is unclear what the appropriate population of the contaminating fast O atoms might be. The ECT-HOPE observations suggest a range of energies for the incoming O^+, which would produce a range of O atoms in speed. Some of these fast O atoms would generate further fast O through momentum transfer with slower O. A detailed analysis extending the previous work of *Ishimoto et al.* [1994] is needed, accounting for the instrument properties of the FPIs and how they would observe the effects of this contamination under different geomagnetic activity levels. Such a study would also allow for the development of improved analysis routines to be able to extract the actual thermospheric properties from storm time observations or, at least, provide bounds on increased error bars on the horizontal thermospheric wind and temperature estimates due to the hypothesized contamination.

While the perspective of the Earth geospace system presented in the introduction regarding the transport of heated air from the polar region to midlatitudes is still likely to be true, this view could now be somewhat confused. The previous work based on FPIs had not allowed for the possible role of spectral contamination of the thermalized spectral line profile. As a consequence, if the hypothesized contamination is, indeed, occurring, previous results derived from similar ground-based FPIs observing the 630.0 nm emission during storm times and analyzed assuming a single population of 630.0 nm photons regarding the increased transport of heated air from the polar region to midlatitudes are called into question by the NATION results presented here. A preliminary investigation through the NATION database from 2013 indicates that this spectral contamination effect (as indicated by sustained apparent downward winds) is present to a lesser degree in several of the other storms captured to date. Deducing the actual bulk thermospheric flow from the effects of spectral contamination is critical to guide the development and validate models used to study the upper atmosphere under storm conditions.

References

Anderson, C., T. Davies, M. Conde, P. Dyson, and M. J. Kosch (2011), Spatial sampling of the thermospheric vertical wind field at auroral latitudes, *J. Geophys. Res.*, *116*, A06320, doi:10.1029/2011JA016485.

Anderson, C., M. Conde, and M. G. McHarg (2012), Neutral thermospheric dynamics observed with two scanning Doppler imagers: 2. Vertical winds, *J. Geophys. Res.*, *117*, A03305, doi:10.1029/2011JA017157.

Acknowledgments

Work at the University of Illinois at Urbana-Champaign, Clemson University, and University of Michigan was supported by the National Science Foundation CEDAR grants AGS-1138998, AGS-1138931, and AGS-1138938, respectively. B.J.H. was supported by the National Science Foundation Graduate Research Fellowship under grant DGE-1144245. Data analysis at Boston University was supported by the National Science Foundation grant OPP-1246423. The Millstone FPI is supported by the National Science Foundation's Aeronomy program. The authors are grateful to the Pisgah Astronomical Research Institute (PARI) and Eastern Kentucky University for their support of the FPI observations. PARI is a not-for-profit foundation with a 200 acre campus in Western North Carolina dedicated to scientific research and education. Eastern Kentucky University is a regional comprehensive university located in Richmond, KY, with a service area including much of the eastern part of the state, the center of Appalachia. The operation of the instrument at Virginia Tech is supported by the Institute for Critical Technologies and Applied Science at Virginia Tech. The authors acknowledge data from the Van Allen Probes ECT-HOPE instrument (http://www.rbsp-ect.lanl.gov/) and discussions with the broader team. The *Dst* data used were obtained from the World Data Center for Geomagnetism in Kyoto, Japan. The *Kp* data used were obtained from the GeoForschungsZentrum Potsdam. The FPI data are available from the Madrigal Database or can be made available by the authors, upon request. The authors thank Peter Sherwood (Interactive Technology) for his contributions toward the development of the FPI data collection software utilized in these measurements. We are grateful to Xiahua Fang for discussions on precipitating ions.

Alan Rodger thanks the reviewers for their assistance in evaluating this paper.

Buonsanto, M. (1999), Ionospheric storms—A review, *Space Sci. Rev.*, *88*(3–4), 563–601.
Burnside, R. G., F. A. Herrero, J. W. Meriwether, and J. C. G. Walker (1981), Optical observations of thermospheric dynamics at Arecibo, *J. Geophys. Res.*, *86*(A7), 5532–5540, doi:10.1029/JA086iA07p05532.
Daglis, I. A., R. M. Thorne, W. Baumjohann, and S. Orsini (1999), The terrestrial ring current: Origin, formation, and decay, *Rev. Geophys.*, *37*(4), 407–438, doi:10.1029/1999RG900009.
Deng, Y., A. D. Richmond, A. J. Ridley, and H.-L. Liu (2008), Assessment of the non-hydrostatic effect on the upper atmosphere using a general circulation model (GCM), *Geophys. Res. Lett.*, *35*, L01104, doi:10.1029/2007GL032182.
Earle, G., R. Davidson, R. Heelis, W. Coley, D. Weimer, J. Makela, D. Fisher, A. Gerrard, and J. Meriwether (2013), Low latitude thermospheric responses to magnetic storms, *J. Geophys. Res. Space Physics*, *118*, 3866–3876, doi:10.1002/jgra.50212.
Fuller-Rowell, T., M. Codrescu, R. Roble, and A. Richmond (1997), How does the thermosphere and ionosphere react to a geomagnetic storm? *Geophys. Monogr. Ser.*, *98*, 203–225.
Funsten, H., et al. (2013), Helium, Oxygen, Proton, and Electron (HOPE) mass spectrometer for the radiation belt storm probes mission, *Space Sci. Rev.*, *179*, 423–484, doi:10.1007/s11214-013-9968-7.
Gonzalez, W., J. Joselyn, Y. Kamide, H. Kroehl, G. Rostoker, B. Tsurutani, and V. Vasyliunas (1994), What is a geomagnetic storm? *J. Geophys. Res.*, *99*(A4), 5771–5792.
Hampton, D. L., J. W. Meriwether, M. F. Larsen, A. J. Ridley, and M. G. Conde (2012), *Sustained Vertical Thermospheric Winds in the Auroral Zone,* no. SA22A-02 in 2012 Fall Meeting, AGU, San Francisco, Calif.
Harding, B. J., T. W. Gehrels, and J. J. Makela (2014), A nonlinear regression method for estimating neutral wind and temperature from Fabry-Perot interferometer data, *Appl. Opt.*, *53*(4), 666–673, doi:10.1364/AO.53.000666.
Hays, P., and R. Roble (1971), Direct observations of thermospheric winds during geomagnetic storms, *J. Geophys. Res.*, *76*(22), 5316–5321.
Hernandez, G. (1982), Vertical motions of the neutral thermosphere at midlatitude, *Geophys. Res. Lett.*, *9*(5), 555–557, doi:10.1029/GL009i005p00555.
Hernandez, G., and R. Roble (1976), Direct measurements of nighttime thermospheric winds and temperatures. 2. Geomagnetic storms, *J. Geophys. Res.*, *81*(28), 5173–5181.
Hernandez, G., and R. Roble (1984), Nighttime variation of thermospheric winds and temperatures over fritz peak observatory during the geomagnetic storm of March 2, 1983, *J. Geophys. Res.*, *89*(A10), 9049–9056.
Hickey, M. P., P. G. Richards, and D. G. Torr (1995), New sources for the hot oxygen geocorona: Solar cycle, seasonal, latitudinal, and diurnal variations, *J. Geophys. Res.*, *100*, 17,377–17,388, doi:10.1029/95JA00895.
Holton, J. R. (1972), *An Introduction to Dynamic Meteorology*, Academic Press, New York.
Hubert, B., J.-C. Gérard, T. L. Killeen, Q. Wu, D. V. Bisikalo, and V. I. Shematovich (2001), Observation of anomalous temperatures in the daytime O(1D) 6300Å thermospheric emission: A possible signature of nonthermal atoms, *J. Geophys. Res.*, *106*(A7), 12,753–12,764, doi:10.1029/2000JA900122.
Ishii, M., M. Conde, R. W. Smith, M. Krynicki, E. Sagawa, and S. Watari (2001), Vertical wind observations with two Fabry-Perot interferometers at Poker Flat, Alaska, *J. Geophys. Res.*, *106*(A6), 10,537–10,551, doi:10.1029/2000JA900148.
Ishimoto, M., G. J. Romick, and C. I. Meng (1992), Energy distribution of energetic O^+ precipitation into the atmosphere, *J. Geophys. Res.*, *97*(A6), 8619–8629, doi:10.1029/92JA00228.
Ishimoto, M., G. J. Romick, and C. I. Meng (1994), Model calculation of atmospheric emission caused by energetic O^+ precipitation, *J. Geophys. Res.*, *99*(A1), 435–447, doi:10.1029/93JA01148.
Keika, K., L. M. Kistler, and P. C. Brandt (2013), Energization of O^+ ions in the Earth's inner magnetosphere and the effects on ring current buildup: A review of previous observations and possible mechanisms, *J. Geophys. Res. Space Physics*, *118*, 4441–4464, doi:10.1002/jgra.50371.
Kerr, R. B. (2014), Redline Instrument Description, retrieved from http://neutralwinds.com/redlinedescribe.html.
Kharchenko, V., A. Dalgarno, and J. L. Fox (2005), Thermospheric distribution of fast O(1D) atoms, *J. Geophys. Res.*, *110*, A12305, doi:10.1029/2005JA011232.
Larsen, M. F., and J. W. Meriwether (2012), Vertical winds in the thermosphere, *J. Geophys. Res.*, *117*, A09319, doi:10.1029/2012JA017843.
Link, R., and L. L. Cogger (1988), A reexamination of the O I 6300-A nightglow, *J. Geophys. Res.*, *93*(A9), 9883–9892, doi:10.1029/JA093iA09p09883.
Makela, J. J., J. W. Meriwether, A. J. Ridley, M. Ciocca, and M. W. Castellez (2012), Large-scale measurements of thermospheric dynamics with a multisite Fabry-Perot interferometer network: Overview of plans and results from midlatitude measurements, *Int. J. Geophys.*, *2012*(3), 1–10, doi:10.1155/2012/872140.
Meriwether, J. (2008), Thermospheric dynamics at low and mid-latitudes during magnetic storm activity, *Geophys. Monogr. Ser.*, *181*, 201–219.
Nicolls, M. J., S. L. Vadas, J. W. Meriwether, M. G. Conde, and D. Hampton (2012), The phases and amplitudes of gravity waves propagating and dissipating in the thermosphere: Application to measurements over Alaska, *J. Geophys. Res.*, *117*, A05323, doi:10.1029/2012JA017542.
Prölss, G. W. (1997), Magnetic storm associated perturbations of the upper atmosphere, *Geophys. Monogr. Ser.*, *98*, 227–241.
Rees, D., R. Smith, P. Charleton, F. McCormac, N. Lloyd, and A. Steen (1984), The generation of vertical thermospheric winds and gravity waves at auroral latitudes—I. Observations of vertical winds, *Planet. Space Sci.*, *32*(6), 667–684, doi:10.1016/0032-0633(84)90092-8.
Rishbeth, H., T. J. Fuller-Rowell, and A. S. Rodger (1987), F-layer storms and thermospheric composition, *Phys. Scr.*, *36*(2), 327–336, doi:10.1088/0031-8949/36/2/024.
Schmitt, G., V. Abreu, and P. Hays (1981), Non-thermal O(1D) produced by dissociative recombination of O_{2^+}: A theoretical model and observational results, *Planet. Space Sci.*, *29*(10), 1095–1099, doi:10.1016/0032-0633(81)90008-8.
Sharp, R. D., R. G. Johnson, and E. G. Shelley (1976a), The morphology of energetic O^+ ions during two magnetic storms: Temporal variations, *J. Geophys. Res.*, *81*(19), 3283–3291, doi:10.1029/JA081i019p03283.
Sharp, R. D., R. G. Johnson, and E. G. Shelley (1976b), The morphology of energetic O^+ ions during two magnetic storms: Latitudinal variations, *J. Geophys. Res.*, *81*(19), 3292–3298, doi:10.1029/JA081i019p03292.
Shelley, E. G., R. G. Johnson, and R. D. Sharp (1972), Satellite observations of energetic heavy ions during a geomagnetic storm, *J. Geophys. Res.*, *77*(31), 6104–6110, doi:10.1029/JA077i031p06104.
Shematovich, V., J.-C. Gérard, D. V. Bisikalo, and B. Hubert (1999), Thermalization of O(1D) atoms in the thermosphere, *J. Geophys. Res.*, *104*(A3), 4287–4295, doi:10.1029/1998JA900154.
Sipler, D., M. Biondi, and M. Zipf (1995), Vertical winds in the midlatitude thermosphere from Fabry-Perot interferometer measurements, *J. Atmos. Terr. Phys.*, *57*(6), 621–629, doi:10.1016/0021-9169(94)00102-T.

Sipler, D. P., and M. A. Biondi (1979), Midlatitude F region neutral winds and temperatures during the geomagnetic storm of March 26, 1976, *J. Geophys. Res.*, *84*(A1), 37–40.

Sipler, D. P., and M. A. Biondi (2003), Simulation of hot oxygen effects on ground-based Fabry-Perot determinations of thermospheric temperatures, *J. Geophys. Res.*, *108*(A6), 1260, doi:10.1029/2003JA009911.

Smith, R., and G. Hernandez (1995), Vertical winds in the thermosphere within the polar cap, *J. Atmos. Terr. Phys.*, *57*(6), 611–620, doi:10.1016/0021-9169(94)00101-S.

Smith, R. W. (1998), Vertical winds: A tutorial, *J. Atmos. Sol. Terr. Phys.*, *60*(14), 1425–1434, doi:10.1016/S1364-6826(98)00058-3.

Space Weather Prediction Center (2013), Space Weather Anonymous FTP Server, retrieved from http://www.swpc.noaa.gov/ftpdir/warehouse/2013/2013_RSGA.tar.gz.

Spencer, N. W., R. F. Theis, L. E. Wharton, and G. R. Carignan (1976), Local vertical motions and kinetic temperature from AE-C as evidence for aurora-induced gravity waves, *Geophys. Res. Lett.*, *3*(6), 313–316, doi:10.1029/GL003i006p00313.

Torr, M., and D. Torr (1979), Energetic oxygen: A direct coupling mechanism between the magnetosphere and thermosphere, *Geophys. Res. Lett.*, *6*(9), 700–702.

Torr, M., D. Torr, R. Roble, and E. Ridley (1982), The dynamic response of the thermosphere to the energy influx resulting from energetic O^+ ions, *J. Geophys. Res.*, *87*, 5290–5300.

Torr, M. R., J. C. G. Walker, and D. G. Torr (1974), Escape of fast oxygen from the atmosphere during geomagnetic storms, *J. Geophys. Res.*, *79*(34), 5267–5271, doi:10.1029/JA079i034p05267.

weatherunderground.com (2013), Weather History for Blacksburg, VA, *Weather Underground*, retrieved from http://www.wunderground.com/history/airport/KBCB/2013/10/2/DailyHistory.html?req_city=NA&req_state=NA&req_statename=NA&MR=1.

Welling, D., and A. Ridley (2010), Exploring sources of magnetospheric plasma using multispecies MHD, *J. Geophys. Res.*, *115*, A04201, doi:10.1029/2009JA014596.

Wilson, G. R., and T. E. Moore (2005), Origins and variation of terrestrial energetic neutral atoms outflow, *J. Geophys. Res.*, *110*, A02207, doi:10.1029/2003JA010356.

Yee, Y. H., J. W. Meriwether, and P. B. Hays (1980), Detection of a corona of fast oxygen atoms during solar maximum, *J. Geophys. Res.*, *85*(A7), 3396–3400, doi:10.1029/JA085iA07p03396.

Yigit, E., A. J. Ridley, and M. B. Moldwin (2012), Importance of capturing heliospheric variability for studies of thermospheric vertical winds, *J. Geophys. Res.*, *117*, A07306, doi:10.1029/2012JA017596.